

Studying the Scattering of Electromagnetic Wave by a Composite 3D Model at Terahertz Frequencies

Mayuri Kashyap¹, Aparajita Bandyopadhyay², and Amartya Sengupta³

¹ *University of Queensland – Indian Institute of Technology, Delhi Academy of Research (UQIDAR), India*

² *Joint Advanced Technology Center, Indian Institute of Technology Delhi, New Delhi, India.*

³ *Department of Physics, Indian Institute of Technology Delhi, New Delhi, India.*

Corresponding Author: amartya@physics.iitd.ac.in

Abstract: Structural inhomogeneity, microscopic variations in material density and compositional fluctuations inherent in biological samples result in strong scattering of the incident radiation. Rigorous scattering solutions available in literature[1-2] based on Rayleigh, Mie theories however, are limited by many assumptions, such as regular geometric pattern, independent scattering centers; and neglect the effects of multiple scattering even though each particle is also exposed to radiation scattered by other particles. In the present work, scattering of electromagnetic wave by composite 3D models in Terahertz (THz) region is explored. The structures are modelled based on biological samples for understanding the nature of interaction, scattering and for identifying the mode of configuration (reflection/transmission) of experimental setup for optimal data acquisition based on a specific frequency range.

Keywords: Electromagnetic scattering, Terahertz, compound model, Far-field

Introduction

Bridging the gap between the far-infrared (FIR) and microwave regions of the electromagnetic (EM) spectrum lies the Terahertz (THz) region, ranging from 0.2 THz (~1.5mm) to 10 THz (~30 μ m).[1] THz radiation has always been present since Big Bang, [2] with human bodies also acting as a source of Terahertz. However, a major surge of activity in this technology was observed since the late 1980s, with the development of femtosecond laser sources to both generate and detect freely propagating THz pulse [3]. Subsequently, the development of THz sources, detectors and systems has seen an upsurge as to tap

its full potential in the promised fields of astrophysics, plasma physics, solid state physics, communication, spectroscopy, imaging and biomedical science to name a few. [3]

Because of its weak photon energy (~ 0.83 meV – 4.14 meV), THz is non-ionizing and is thus, innocuous to biological matter. Moreover, in this energy range, the collective motions of many intermolecular vibrational modes are active, making it suitable for identifying the material composition through their unique spectral fingerprints. THz can penetrate into most dielectrics (wood, paper, etc.) which are usually opaque in the visible range but, is absorbed in the presence of polar materials (water). The later property is substantial as it allows THz to be highly sensitivity to the presence of water, critical in many applications monitoring the hydration level of the system [4]. Exploiting such unique properties of THz, technology has been developed for its application in the inspection of paint layers, plastics, industrial quality control, hydration monitoring, security, environmental control, gas sensing, and forensics among others. [5]

The performance of THz field is however, observed to be considerably affected by the classical problem of scattering. Scattering itself is responsible for the occurrence of few other phenomena, be it the reason for the blue colour of sky in the visible range [7, 8] or the detection of aircraft in the microwave. Wave propagation and scattering in oceans, atmosphere and random media has been discussed in [9] and is a topic of considerable interest in the fields of optics, acoustics and biological media.

The scattered field in the THz region is now utilized in scattering-type SNOM for extraction of dielectric

information [10] and in dark field imaging to increase the contrast of edges [11]. These are special occurrences which have exploited the scattered field, but for normal scenarios, it acts as a limiting factor. Scattering attenuates the resultant field, and because of low power generated from the sources (the technology yet being in its developing stage), the effect of scattering is significant in the THz region. The wavelength of THz is in the sub-millimeter range, longer than that in the visible or infrared region. Because of this, scattering induces blurring effect in the images and introduces artifacts unlike in any other optical imaging method [4].

Most of the rigorous theoretical scattering solutions available deal only with regular geometries like spheres and cylinders in free space [7, 8] and avoid the case of dependent scattering and multiple scattering because of the increased complexity. A few analytical solutions are present for arbitrary geometries like cylindrical wedges, spheroids, discussed in [12, 13].

But, biological media (leaf, skin, petals), food materials, packaging material, pharmaceutical drugs, powered substances which act as scattering centers cannot be considered to fulfill the above criteria as they are inhomogeneous, both in structure and composition. The possible number of variations of each type is again countless. The analysis of scattered field for such scenarios thus, becomes challenging and yet, to correctly determine the material parameters, it is an important process.

The present work focuses on analysis of scattered field from such a surface using COMSOL Multiphysics®, which provides a flexible and reliable platform to model such compound 3D structures. COMSOL, also includes inbuilt feature for far-field domain calculation which allows the simulation of the scattered far-field, aiding to understand the scattered field behaviour for specific frequency ranges.

Theory

When an incident electromagnetic (EM) wave, propagating in a medium, interacts with a molecule, or dielectric particle (or region), the electric field of the wave polarizes the particle. The molecules in the

particle couple and oscillate with the electric field of the wave and thus, radiate EM wave in all directions. This phenomenon is known as scattering.

Reradiating the incident wave redistributes the energy and thus, the intensity along the original direction of propagation is attenuated. [14]

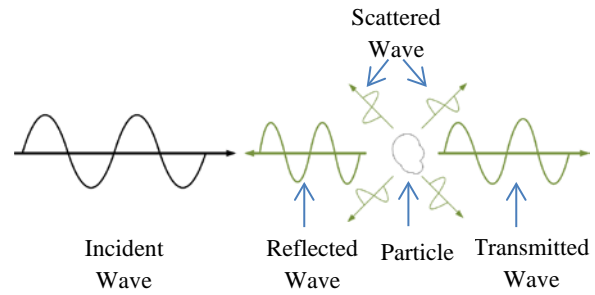


Figure 1: Scattering of EM wave by irregular particle. Resultant intensity is attenuated due to scattering of light in random direction and absorption by particle.

The cases of reflection, diffraction and transmission are special cases of scattering where the direction of irradiation is regular and follows the general laws of physics such as laws of reflection, refraction. It is the irradiation in random direction which causes hindrance to the actual measurement of resultant field vector. The term, scattering in this paper, is only concerned with this later phenomenon.

Scattering along with absorption by the particle (energy transformed into another form), is responsible for the total loss of intensity of incident radiation, and together, these two factors are known as extinction. [8]

$$\text{Scattering} + \text{Absorption} = \text{Extinction}$$

Here, we concern ourselves only with the elastic scattering of incident radiation, where the kinetic energy of the system is conserved but the direction of propagation is modified. Scattering is dependent on the size, shape, orientation and composition of the particle. Thus, fluctuation in material density, refractive index, surface topology all contribute towards changes in the scattered field.

Scattering of EM wave can be classified broadly into three categories: Rayleigh, Mie and geometric scattering based on a dimensionless factor, size parameter. The size parameter, a is proportional to the ratio the particle size and incident wavelength and can be given as:

$$a = 2\pi r/\lambda$$

where λ is the wavelength of incident wave and r is for the determining size of the scattering particle (radius in case of spherical particle).

$$\text{Scattering} = \begin{cases} \text{Rayleigh} & a \ll 1 \\ \text{Mie} & a \approx 1 \\ \text{Geometric} & a \gg 1 \end{cases}$$

The Rayleigh scattering is evident for scatterers when the size of the particle, r is very smaller compared to the incident EM wavelength. Scattering in this domain is often characterized by equivalent scattering in the forward and reverse directions and is often depicted as a sphere of equal volume for a spherical particle.

As the size of the scattering particle becomes comparable to the wavelength, scattering comes under the domain of Mie scattering, named so after Gustav Mie. In this region, the scattering observed is directional in nature with more scattering in the forward region compared to the in the reverse direction.

The domain again changes to geometric scattering when the size parameter becomes very larger than 1 i.e. when the particle size is considerably larger than the wavelength. The phenomenon is then governed by laws of geometrical optics and such an interaction is usually not described as scattering.

Computational Method

In electromagnetic wave scattering, the total wave decomposes into incident and scattered wave. A good measure of the scattering field is the scattering cross section area and its formulations are based on Maxwell's equation. [7,8,16]

The energy redistribution due to scattering of EM wave can be obtained from the Maxwell's equations:[15]

$$\nabla \times \mathbf{E} = -\mu \frac{d\mathbf{H}}{dt} \quad (1)$$

$$\nabla \times \mathbf{H} = \sigma \mathbf{E} - \varepsilon \frac{d\mathbf{E}}{dt} \quad (2)$$

Taking volume integral of the transformed equations and applying divergence theorem gives:

$$\oint_S (\mathbf{E} \times \mathbf{H}) \cdot d\mathbf{S} = -\frac{\partial}{\partial t} \int_v \left[\frac{1}{2} \varepsilon E^2 + \frac{1}{2} \mu H^2 \right] dv - \int_v \sigma E^2 dv \quad (3)$$

Equation (3) is referred to as the Poynting's Theorem which states the net power flowing out of a given volume, v is equal to the time rate of decrease in energy stored within the volume minus the losses.

The term, $\mathcal{P} = \oint_S (\mathbf{E} \times \mathbf{H}) \cdot d\mathbf{S}$ is known as the Poynting vector and it represents the energy flux density (energy per unit area per unit time).

For all practical purposes, this instantaneous value is time averaged for time harmonic fields which gives the magnitude of irradiance (energy flux per unit area) of the incident wave.

$$\mathcal{P}_{avg} = \frac{1}{2} \text{Re}[\mathbf{E} \times \mathbf{H}^*] \quad (4)$$

Again, one of the relations for plane wave derived from Maxwell's equation states:

$$\mathbf{H} = \frac{1}{\eta} (\hat{\mathbf{k}} \times \mathbf{E}) \quad (5)$$

$$\text{Or, } \eta = \sqrt{\mu/\varepsilon} \quad (6)$$

where $\hat{\mathbf{k}}$ is the unit vector along the direction of wave propagation and η is the wave impedance, μ is the permeability and ε is the permittivity of the material.

The irradiance can thus be given as:

$$\mathcal{J}_i = |\mathcal{P}_{avg}| = \frac{1}{2\eta} |E|^2 \quad (7)$$

The scattering cross section, CSA_{sca} is calculated by integrating the relative Poynting vector over the particle surface. For absorption cross section, CSA_{abs} , the energy dissipated in the volume of the particle is calculated. The extinction cross-section, CSA_{ext} gives a measure of the energy attenuated due to scattering

and absorption and given by the superposition of CSA_{sca} and CSA_{abs} .

$$C_{ext} = C_{sca} + C_{abs} \quad (8)$$

$$\text{Or, } \frac{W_{ext}}{J_i} = \frac{W_{sca}}{J_i} + \frac{W_{abs}}{J_i} \quad (9)$$

where W_{sca} and W_{abs} are the rate at which electromagnetic energy is scattered and absorbed by the particle and J_i the incident irradiation.

In COMSOL, the wave equation for the scattered field is governed by the equation:

$$\nabla \times \left(\frac{\nabla \times \mathbf{E}}{\mu_r} \right) - k^2 \left(\mu_r - \frac{i\sigma}{\omega\epsilon_0} \right) \mathbf{E} = 0 \quad (10)$$

where \mathbf{E} is the incident electric field for the planar wave. For simulation, the electric field considered, is x-polarized and of the form:

$$\mathbf{E} = E_0 \cdot \exp(ikz) \hat{x} \quad (11)$$

E_0 : amplitude of incident electric field (1 V/m),
 \mathbf{k} is the incident wave propagation vector with

$$k = |\mathbf{k}| = 2\pi/\lambda$$

Simulation: Model and Method

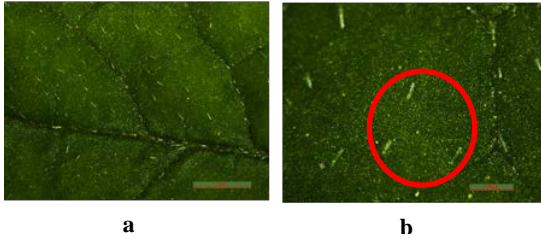


Figure 2: Microscopic images of bitter gourd leaf showing presence of trichomes acquired with Laica M205C microscope of resolution a) 2mm b) 500µm. The red circle highlights the area under present simulation study. Leaf thickness: 0.12mm

A peculiar case of scattering is observed in the THz region for leaves of certain plants because of the presence of thin, hair-like structures, called trichomes on its epidermal surface (Figure 2).

To analyze the effect of scattering by such surfaces, models (Table 1-a, Table 1-b) in hierarchical order of increasing complexity were developed with the size

and structure of final model (Model 2) comparable to highlighted segment of Figure 2 b).

Table 1-a: Simulation Model Structures and Description-Model 1. For base, height= 0.1, radius= 0.12; for hemispheres, radius=0.03; Dimensions are in mm.

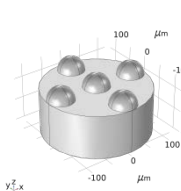
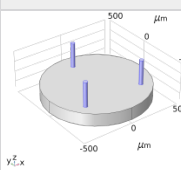
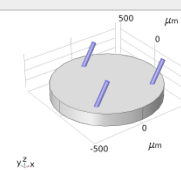
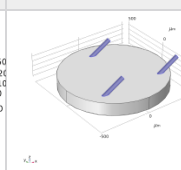
Structure	Model	Description
	Model 1-a	Refractive Index (RI): 3.67 + 0.005i
	Model 1-b	base_RI: 3.95+0.08i hemisphere_RI: 3.67 + 0.005i
	Model 1-c	RI: ref. Table 4

Table 1-b: Simulation Model Structures and Description-Model 2. For leaf, height= 0.12, radius= 0.5; for trichome: height= 0.24, radius= 0.02. Dimensions are in mm.

Model 2-a	Model 2-b	Model 2-c
		
Inclination of Trichome: 0° RI: ref. Table4	Inclination of Trichome: 30° RI: ref. Table4	Inclination of Trichome: 60° RI: ref. Table4

The model was designed in COMSOL, with the Electromagnetic Waves, Frequency Domain interface of Wave Optics module which supports the modelling of 3D structures, scattering field formulation and far field analysis for electromagnetic waves at optical frequencies. To contain the solution within a region of interest, periphery of the model was limited by a sphere of perfectly matching layer (PML) having finite thickness. PML does not affect the solution and allows the EM wave to behave as if the source and sink are at infinity. Proper boundary conditions, defining the particle, the PML layer, area of surface integral and volume integral for proper calculation of scattering cross section and absorbing cross sections were selected.

COMSOL does the far-field calculation on the inner boundary of the PML. With the surrounding medium as air, the complete model is discretized using Physics controlled fine mesh, dependent on the wavelength. The scattered field formulation and far-field domain available for the selected interface allows the analysis of the relative electric field and give the scattered far-field 3D plots.

Results and Discussion

Model 1 and Model 2 were analyzed for certain frequencies in the range of 0.2-2.2 THz and 0.2-1 THz. The study was however, not parameterized over the frequency range since the radius of PML was considered to vary with frequency. This was done to decrease the computational cost on the system (smaller wavelengths) and to allow at least one complete wavelength of the incident planar wave inside the PML (for longer wavelengths).

The scattering cross sections and scattered far-fields for Model 1-a and Model 1-b, along with its input parameters are presented in Table 2 and Table 3.

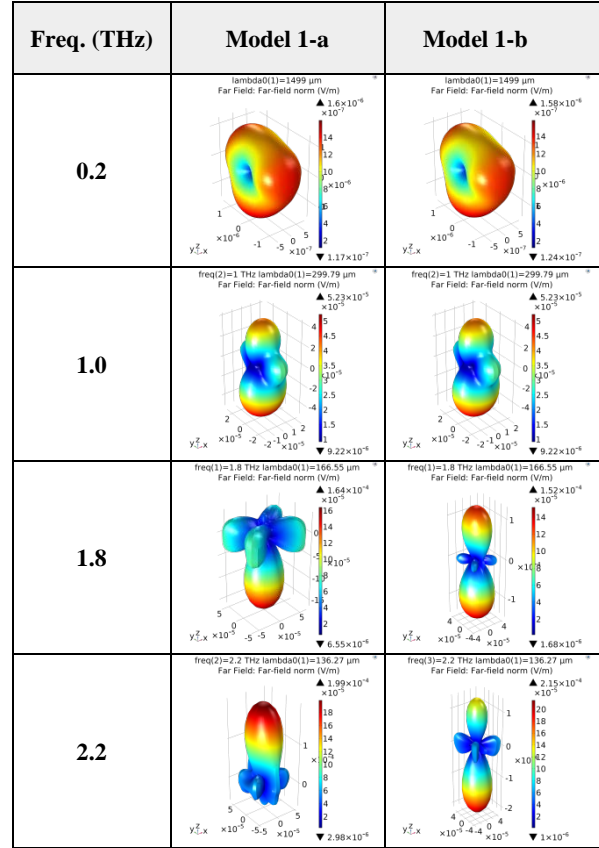
Table 2: Scattering cross-section (m^2) for model 1-a and model 1-b, with frequency.

Model	Freq. (THz)	λ (μm)	PML radius(μm)	SCA ($10^{-8} m^2$)
Model 1-a	0.2	1499	1560	0.5135
	1.0	299.79	720	8.3472
	1.8	166.55	480	12.779
	2.2	136.27	480	5.6013
Model 1-b	0.2	1499	1560	0.5633
	1.0	299.79	720	8.3472
	1.8	166.55	480	6.9774
	2.2	136.27	480	6.8164

At lower frequency, the scattering is observed to be almost uniform along the forward and backward directions, showing a transition from the Rayleigh towards the Mie domain. With increase in frequency (\sim decrease in wavelength), the size parameter starts increasing towards 1 and a definite directional pattern is observed, the forward scattering increasing constantly. The scattering cross-sectional area also increases with increasing frequency. However, a

directional change is observed for Model 1-a, from majorly forward scattering at 1.8 THz to backward scattering at 2.2 THz.

Table 3: Scattered far-field for model 1-a and model 1-b with frequency



The scattering cross-sectional area also decreases and we can infer some other material dependent radiative phenomena such as resonance effect instigating the change. It is important to note that that the scattering is not unidirectional (presence of side lobes); Poutrina et.al in their work [17] presents switching between forward and backward directionality due to change in excitation wavelength. A similar trend is observed for Model 1-b, however, the structure consisting of two different materials for base and particles (as compared to only one material for Model 1-a with lower refractive index) does not show such a feature for our interested frequency range. But, the scattering cross-section does reduce by a very small margin.

To analyze the effect of embedded hemispheres in Model 1, a similar simulation was done for only the base (material same as for Model 1-b) and observed that without the particles, the scattering was more uniform, thus, showing the effect of structural inhomogeneity on scattering, even for low frequency (or, long wavelength).

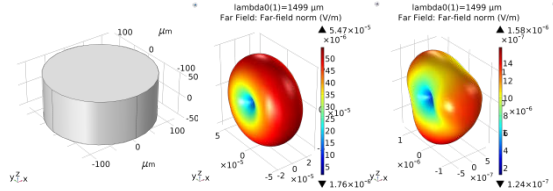


Figure 3: At 0.2 THz, FF for geometry in a) is given in b). c) FF Pattern for Model 1-b; FF at b) is more uniform

With these results, the size and structure of model was increased to match the leaf structure in Figure 2b. Unlike as in model 1, the refractive indices are also varied in the range of 0.2- 1 THz. To depict the slanting trichomes, scattering is analyzed for the trichomes modelled at an angle of 0°, 30° and 60°. The modelling parameters and scattering far-field and

Frequency (THz) →	0.2	0.6	1
λ (μm)	1499	500	299.79
RI: Leaf ($n+ik$)	1.50+0.50i	1.45+0.45i	1.40+0.40i
RI: Trichome ($n+ik$)	1.45+0.45i	1.40+0.40i	1.35+0.35i
PML radius(μm)	3000	2000	2000

Table 4: Input parameters for Model 2. RIs also utilized for Model 1-c, with base as leaf and hemispheres as trichomes.

The RIs considered are approximated from 1.35~1.5 (for real) and 0.35~0.5 (for imaginary), close to RI of actual leaves [18]. To confirm the applicability of deductions from model 2 to other similar structures, the same range of RI is considered for Model 1-c.

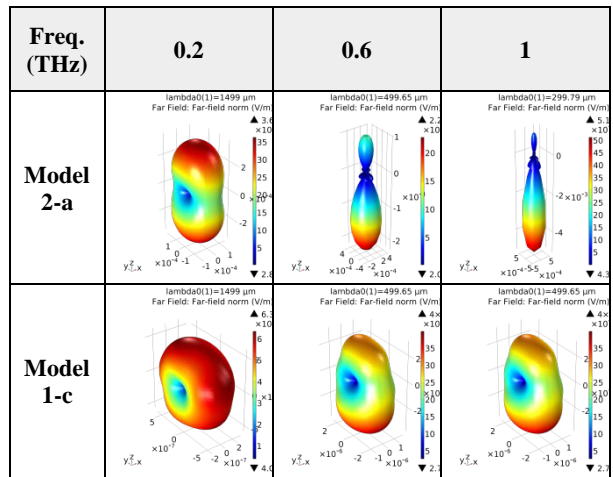
Inclination of the trichomes has almost negligible effect in the measure of scattering cross section (Table 5) and scattered far-field pattern. In lower

frequency, proportion of forward to backward scattering is comparable.

Table 5: Scattering cross-section (m^2) for model 2-a, 2-b, 2-c and model 1-c, with frequency.

Model	Freq. (THz)	SCA (10^{-8}m^2)	Model	Freq. (THz)	SCA (10^{-8}m^2)
Model 2-a	0.2	13.522	Model 2-c	0.2	13.537
	0.6	39.277		0.6	38.975
	1.0	59.817		1.0	59.723
Model 2-b	0.2	13.490	Model 1-d	0.2	0.072
	0.6	39.207		0.6	1.853
	1.0	59.842		1.0	2.599

Table 6: Scattered far field and scattering cross section for Model 2-a and Model 1-c.



With increase in frequency, the scattering cross-section increases; strong directional forward scattering is observed indicating Mie scattering for the higher frequency range. This is true for Model 1-c also, though the directionality is not as strong as for Model 2.

The particle size for Model 2 being larger than Model 1, scattering is significantly large. It is also observed to increase with frequency. This increase is more prominent in the smaller model 1-c with same refractive indices, as the scattering cross-section increases from $7.190 \times 10^{-10} \text{ m}^2$ at 0.2 THz to $1.853 \times 10^{-8} \text{ m}^2$ at 0.6 THz.

Conclusion and Future Work

For use in actual experimental setup, analysis of the obtained results show that for lower frequency (~0.2 THz), the proportion of forward scattering to backscattering is almost equal; so data can be acquired both in reflection or transmission mode with little or negligible effect. On the other hand, for higher frequencies, the scattering increases and it is inevitable that data is acquired in reflection mode as most of the transmitted data is scattered, which leads to attenuation of the resultant electric field in the propagation direction. Also, for same frequency, scattering is significantly large for larger structures.

Besides this direct use of the analysis, the above model is also very much relevant for typical biological samples (leaves, petals, skin, etc.), common chemicals, food samples, patterned semiconductor heterostructures etc.

Acknowledgements

1. Defence Research and Development Organization (DRDO) vide Grant #DFTM/03/3203/M/JATC.
2. Department of Atomic Energy- Board of Research in Nuclear Sciences (DAE-BRNS) vide Grant # 37 (3)/14/01/2016-BRNS/37015.

References

1. R. A. Lewis, *Terahertz Physics*, Cambridge University Press, 2012
2. P.H. Siegel, *IEEE Transactions on Microwave Theory and Techniques*, 50 (2002) 910–928.
3. D. Dragoman, M. Dragoman, *Review: Terahertz fields and applications*, *Progress in Quantum Electronics*, 28 (2004) 1–66
4. Yun-Shik Lee, *Principles of Terahertz Science and Technology*, Springer, 2009
5. Anselm Deninger, *State-of-the-Art Terahertz Systems and Their Applications*, OSA Technical Group Webinar, May 21, 2019
6. Jeremy Pearce, Zhongping Jian, and Daniel M. Mittleman, *Statistics of Multiply Scattered Broadband Terahertz Pulses*, *Physical Review Letter*, Volume 91, Number 4, 043903, 2003
7. C. F. Bohren, D. R. Huffman, *Absorption and Scattering of Light by Small Particles*, Wiley, New York, 1983
8. H. C. van de Hulst, *Light Scattering by Small particles*, Dover, 1981
9. A. Ishimaru, *Wave Propagation and Scattering in Random Media*, Academic Press, New York, 1978
10. Daniel M. Mittleman, *Perspective: Terahertz science and technology*, *J. Appl. Phys.* 122, 230901, 2017
11. Wai Lam Chan, Jason Deibel and Daniel M Mittleman, *Imaging with terahertz radiation*, *Rep. Prog. Phys.* 70, 1325–1379, 2007
12. Fabrizio Frezza, Fabio Mangini, and Nicola Tedeschi, *Introduction to electromagnetic scattering: tutorial*, *J. Opt. Soc. Am. A* 35, 163-173, 2018
13. H. Laurell, J. Hillborg, *Towards a tunable nanometer thick flat lens (Dissertation)*, 2018.
14. S. O. Kasap, *Principles of Electronic Materials and devices*, Second Edition, McGraw-Hill, 2001
15. Matthew N. O. Sadiku, *Elements of Electromagnetics*, New York: Oxford University Press, 2001
16. Sergei Yushanov, Jeffrey S. Crompton, and Kyle C. Koppenhoefer, *Mie Scattering of Electromagnetic Waves*, COMSOL Conference, Boston, 2013
17. Poutrina, Ekaterina & Rose, Alec & Brown, Dean & Urbas, Augustine & Smith, D. (2013). *Forward and backward unidirectional scattering from plasmonic coupled wires*. *Optics express*. 21. 31138-54. 10.1364/OE.21.031138.
18. K. Singh, A. Bandyopadhyay, & A. Sengupta, *Water estimation in plants using Terahertz imaging*, 7th International Conference on Perspective of Vibrational Spectroscopy, BARC (2018)